AdvBokeh: Learning to Adversarially Defocus Blur

Yihao Huang[1], Felix Juefei-Xu[2], Qing Guo[3], Weikai Miao[1], Yang Liu[3,4], Geguang Pu[1,5]

[1]East China Normal University, China, [2]Alibaba Group, USA,
[3]Nanyang Technological University, Singapore, [4]Zhejiang Sci-Tech University, China,
[5]Shanghai Industrial Control Safety Innovation Technology Co., Ltd., China

Abstract

Bokeh effect is a natural shallow depth-of-field phenomenon that blurs the out-of-focus part in photography. In pursuit of aesthetically pleasing photos, people usually regard the bokeh effect as an indispensable part of the photo. Due to its natural advantage and universality, as well as the fact that many visual recognition tasks can already be negatively affected by the 'natural bokeh' phenomenon, in this work, we systematically study the bokeh effect from a new angle, i.e., ***adversarial bokeh attack (AdvBokeh)*** *that aims to embed calculated deceptive information into the bokeh generation and produce a natural adversarial example without any human-noticeable noise artifacts. To this end, we first propose a Depth-guided Bokeh Synthesis Network (DebsNet) that is able to flexibly synthesis, refocus, and adjust the level of bokeh of the image, with a one-stage training procedure. The DebsNet allows us to tap into the bokeh generation process and attack the depth map that is needed for generating realistic bokeh (i.e., adversarially tuning the depth map) based on subsequent visual tasks. To further improve the realisticity of the adversarial bokeh, we propose depth-guided gradient-based attack to regularize the gradient. We validate the proposed method on a popular adversarial image classification dataset, i.e., NeurIPS-2017 DEV, and show that the proposed method can penetrate four state-of-the-art (SOTA) image classification networks i.e., ResNet50, VGG, DenseNet, and MobileNetV2 with a high success rate as well as high image quality. The adversarial examples obtained by AdvBokeh also exhibit high level of transferability under black-box settings. Moreover, the adversarially generated defocus blur images from the AdvBokeh can actually be capitalized to enhance the performance of SOTA defocus deblurring system, i.e., IFAN.*

1. Introduction

In photography, the shallow depth-of-field (DoF) effect or the bokeh effect is an important technique to generate aesthetically pleasing photographs. The images with the bokeh effect draw the attention of the viewers by primarily blurring the out-of-focus parts of the images while keeping the focused parts sharply. This effect can wash out unnecessary image details such as cluttered background, which can save the viewers from the messy information of the images and emphasize the salient themes such as foreground person or object of the images. However, "natural bokeh" (such as examples shown in Fig. 1 top part) as a common and natural phenomenon in photography may already reveal vulnerabilities in various visual image understanding tasks. For example, the natural bokeh effect may degrades the visual tasks [6,33,36,43,46] such as image classification [6,33,43], object recognition [46], object detection [36], *etc*.

Due to its natural advantage and universality in photos,

Figure 1. (Top) Real-world bokeh examples taken with DSLR at various focal lengths and f-stops. (Bottom) Adversarial bokeh examples produced by the proposed *AdvBokeh* can fool ResNet50 image classification.

as well as potential adverse effects on multifarious visual tasks, in this work, we aim to systematically study the bokeh effect from a new angle, *i.e*., ***adversarial bokeh attack (AdvBokeh)*** that is purposed to add calculated and deceptive information into the bokeh generation procedure and produce a natural bokeh-like adversarial example without any human-noticeable noise artifacts. Adversarial bokeh examples are shown in Fig. 1 bottom part.

To allow this to happen, we need to tap into the bokeh rendering mechanism and understand the inner workings. There are mainly two ways to produce a bokeh effect, which is either generated optically or through computational photography methods. To physically and optically produce the bokeh effect, usually fast lenses (*e.g*., small f-stop prime lenses used in Fig. 1) with large aperture in tandem with high-end digital single-lens reflex (DSLR) cameras or the latest digital single-lens mirrorless (DSLM) cameras are needed. The high barrier of entry has limited this option largely to professionals. On the other hand, the latest smartphone manufacturers have tried to enable a computational photography way of generating realistic bokeh effect on consumer-level cell phone products, which strongly drives research in this direction. The early works [39, 40, 52] put emphasis on portrait photos, which neglects the bokeh effect generation for images in the wild. Soon afterward, to extend the scope of applicable scenarios, some works propose methods for wild scene bokeh effect rendering [34, 35, 47, 48] and "AIM 2019 Challenge on Bokeh Effect Synthesis" competitions [22] have been organized to foster the development of computational photography-based bokeh effect synthesis. Recently, two state-of-the-art methods [5, 21] have obtained a highly realistic bokeh effect with a well-designed DNN and multi-stage training.

However, the aforementioned methods mainly suffer from one or more of the following three problems during the bokeh effect synthesis: ❶ The multi-stage training procedure is time-consuming. ❷ Most of them can only focus on the foreground objects and lack the refocusing flexibility. That is, they can not generate bokeh effect images that focus on background objects. ❸ The bokeh effect generated by them has an obvious distinction from the realistic one. To be more specific, the light spots in the all-in-focus images should become lens flares in bokeh images. Most of the previous methods do not achieve this effect.

To this end, in this paper, we propose a novel ***Depth-guided Bokeh Synthesis Network (DebsNet)*** that is able to flexibly and realistically synthesize, refocus, and adjust the level of bokeh of the image, with a one-stage training procedure, and without using any specialized hardware. Specifically, the proposed method achieves high-realisticity bokeh effect rendering by fusing the all-in-focus image and the defocus blurred versions of it simultaneously. The blurred versions of the all-in-focus image, which we term as the blur templates, are generated by disk blur with various kernel sizes and gamma correction. Our method has four main advantages: ❶ The network is trained end-to-end in one stage, which is time-efficient. ❷ The depth guidance offers the method the flexibility to refocus onto arbitrary objects according to the depth map. ❸ Through well-designed preprocessing of the blur templates, the generated bokeh effect can exhibit realistic and aesthetically pleasing lens flare effects. ❹ The degree of bokeh is adjustable for that we can generate blur templates with varying blur degrees.

The proposed DebsNet allows us to dig into the bokeh generation process and adversarially tune the depth map that is needed for generating realistic bokeh based on subsequent visual tasks. To further improve the realisticity of the adversarial bokeh, we propose a depth-guided gradient-based attack to regularize the gradient. We validate the proposed method on a popular adversarial image classification dataset, *i.e*., NeurIPS-2017 DEV, and show that the proposed method can penetrate four state-of-the-art (SOTA) image classification networks *i.e*., ResNet50, VGG, DenseNet, and MobileNetV2 with high success rates as well as high image quality. Moreover, the adversarially generated defocus blur images from the AdvBokeh can actually be capitalized to enhance the performance of SOTA defocus deblurring system, *i.e*., IFAN.

The contributions are summarized as follow:

❶ We propose a novel *Depth-guided Bokeh Synthesis Network (DebsNet)*. The method has the capability to flexibly and realistically synthesize, refocus, and adjust the level of bokeh. The training procedure is one-stage.

❷ We reveal that the "natural bokeh" effect can already negatively impact various visual tasks and then propose the depth-guided bokeh attack, *i.e*., AdvBokeh for image classification tasks by tapping into the bokeh generation process via the proposed DebsNet. The generated bokeh attack images can further improve the performance of defocus deblurring systems, demonstrating that the adversarially learned defocused image can be further capitalized for enhancing downstream visual tasks.

❸ The adversarial attack experiments are conducted on a popular adversarial image classification dataset, showing that the proposed method can penetrate four SOTA image classification networks with high success rates as well as maintain high image quality compared to two SOTA defocus blur synthesis methods. The adversarial examples obtained by AdvBokeh also exhibit high level of transferability under black-box settings. Moreover, the adversarially generated defocus blur images from the AdvBokeh can actually be capitalized to enhance the performance of SOTA defocus deblurring system.

Social impact. We envision that our method could be used in numerous applications including creative uses in the photography or generation of realistic training data. The attack

method, if maliciously used by an adversary, may cause harm to the digital media. The study herewithin attempts to expose potential vulnerabilities of the neural network with the natural photography phenomenon, alerting the researchers to improve the robustness of the neural network.

2. Related Work

DoF rendering. DoF rendering plays an important role in realistic image synthesis. A number of works [15, 27, 42, 50, 53] have tried using ray tracing or light field rendering to synthesis realistic bokeh effect images. Most of these methods need accurate 3D scene information and are time-consuming. To achieve a realistic bokeh effect on single RGB images captured by the monocular camera, early works [39, 40, 52] first take portrait as the target of bokeh effect rendering. To generate realistic portraiture which contains different image rendering styles on foreground and background, Shen *et al*. [40] proposes a fully automatic portrait segmentation technique by utilizing FCN [30]. With the accurate segmentation map, they can easily apply DoF rendering in the background. Shen *et al*. [39] first use trimap labeling which clearly distinct foreground, background and unknown pixels. Then they use an image matting module to further segment foreground and background, which is the expansion of [40]. To get a detailed and accurate depth map, Xu *et al*. [52] first use a learning-based method to achieve a coarse depth map of the input image and then refine it with spatial propagation networks (SPN) [29]. They propose using conditional random field (CRF) [57] and image matting to blur the background of the all-in-focus image. They also use a spatially-variant recursive neural network to learn and accelerate the rendering process. However, the previous methods put emphasis on portrait photos, which neglects the bokeh effect generation for images in the wild.

To expand the application domain of DoF rendering, recently researchers proposed a lot of works [5,21,34,47,48]. Wang *et al*. [48] proposes a neural network with a depth estimation module, a lens blur module and a guided upsampling module to render the bokeh effect on high-resolution images. Wadhwa *et al*. [47] present a system to computationally synthesize bokeh effect images by utilizing a person segmentation network to distinct foreground and background. They also propose an algorithm for dense depth maps generation with dual-pixel auto-focus hardware, which can be used to render wild scene images. Purohit *et al*. [34] propose a method that computes depth map and saliency map first and then uses a densely connected encoder-decoder backbone with a pyramid pooling module to generate spatially-aware dynamic filters to render the bokeh effect. Ignatov *et al*. [21] present a large-scale bokeh dataset named "Everything is Better with Bokeh!" (EBB!), which contains 5K shallow DoF image pairs captured using the Canon 7D DSLR. They propose PyNET-based architecture with multi-stage training to render the bokeh effect. Dutta *et al*. [5] proposes an end-to-end deep multi-scale hierarchical network (DMSHN) for the bokeh effect rendering of images captured from the monocular camera.

These methods suffer from several defects such as lack of refocusing flexibility, require time-consuming multi-stage training, unrealistic bokeh effect, *etc*.

Unrestricted attack. Adversarial attacks that generate L_p-norm perturbations have obvious noises and are now considered unrealistic. Recent works [1,2,7,13,18,38,51] have tried to put emphasis on generating unrestricted adversarial images, which will not raise the suspicion of the people. From this point of view, the unrestricted adversarial images make more sense in practical use scenarios.

The attacks mainly focus on three categories: geometric transformation, color modification and photography effect. A few works exploit image deformations to construct adversarial attacks [1,7,51]. The images do not contain unnatural noise. However, image distortion is not natural when applying to images with straight edges. Some works have tried to do semantic adversarial attacks by modifying the color of the object in the image [2,18,38,56]. However, the colors of some objects in the adversarial attacked images defy common sense and look very fake (*e.g*., yellow river, purple tree, *etc*.). Guo *et al*. [13] propose an adversarial attack method that can generate visually natural motion-blurred adversarial examples, which mimics a type of photographic effect with high fidelity. However, the method did not consider the depth information of the image, and cannot be extended to generating defocus blur.

3. Proposed Depth-guided Bokeh Synthesis

3.1. Motivation

Although existing bokeh effect rendering methods have achieved impressive photography effects, they still face two main problems: ❶ Existing bokeh effect rendering methods mainly design data-driven end-to-end networks by using loss functions such as L_1 loss, SSIM loss, perceptual loss, *etc*., to supervise the training procedure. They hope that the neural network can learn the bokeh effect directly, which ignores the physical principle and may fail when uncovered data appears. For example, they usually introduce some special effects (*e.g*., lens flare) of bokeh that are different from blur. To solve this issue, we regard the bokeh effect rendering as an image blending problem. The blending materials are an all-in-focus image and its blur versions (*i.e*., blur templates). We can generate blur templates that approximate the physical model of bokeh as candidates for blending, which guarantees that the synthetic result is close to the realistic one. ❷ Existing bokeh effect rendering meth-

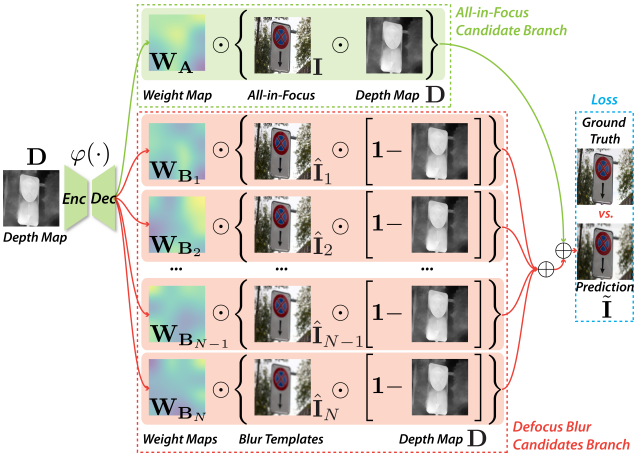

Figure 2. Architectures and training pipeline of *Depth-guided Bokeh Synthesis Network (DebsNet)*. As detailed in §3.2, the encoder-decoder takes depth map as input and generates weight maps. Then the all-in-focus candidate branch and the defocus blur candidates branch use the weight maps to blend the depth-map-guided all-in-focus images and blur templates, obtaining the prediction bokeh image. The network finally calculates the loss by comparing predicted and ground truth bokeh images.

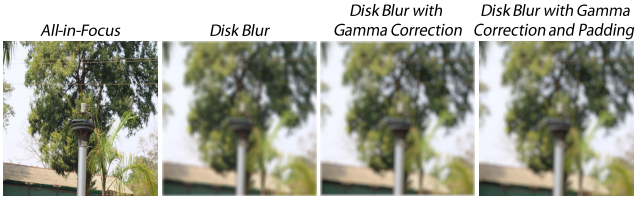

Figure 3. (L-R) all-in-focus image, image with disk blur effect, image with disk blur and gamma correction effect, image with disk blur, gamma correction and padding effect.

Figure 4. (L-R) blur templates with kernel sizes 13, 21, 29, 37.

ods take all-in-focus images as input and learn a mapping function to produce foreground-focus images. This makes them lack the capability of refocusing on the other objects (*e.g.*, background objects). To alleviate this issue, we employ the depth map to guide the fusion of the all-in-focus image and its blur templates. As a result, the network is able to refocus on anywhere of the image according to the adjustable depth map. To summarize, we propose the *Depth-guided Bokeh Synthesis Network (DebsNet)* that has the flexibility of refocus and can render the bokeh effect close to the physical model, to be introduced in §3.2.

3.2. Depth-Map-Aware Bokeh Generation

Given an all-in-focus image $\mathbf{I} \in \mathbb{R}^{H\times W\times 3}$ with intensity range of $[0, 255]$, we first estimate its depth map $\mathbf{D} \in \mathbb{R}^{H\times W}$ with a pre-trained depth estimation network [48]. The intensity of map $\mathbf{D}$ ranges within $[0, 1]$ and the depth value of foreground is close to 1 while the depth value of the background is close to 0. We are able to obtain the blur template $\hat{\mathbf{I}} \in \mathbb{R}^{H\times W\times 3}$ of the all-in-focus image $\mathbf{I}$ with blur template generation operation $\mathcal{T}(\cdot)$ and the kernel size of the disk blur (*i.e.*, k) [37]

$$\hat{\mathbf{I}} = \mathcal{T}(\mathbf{I}, k). \tag{1}$$

We then generate N blur templates $\{\hat{\mathbf{I}}_1, \hat{\mathbf{I}}_2, \ldots, \hat{\mathbf{I}}_N\}$ by $\{\hat{\mathbf{I}}_i\}_{i=1}^N = \{\mathcal{T}(\mathbf{I}, k_i)\}_{i=1}^N$. with N kernel sizes (*i.e.*, $\{k_1, k_2, \ldots, k_N\}$) where $N \geq 1$ depends on the actual situation. Intuitively, we are able to generate blur templates with varying blur degrees according to various kernel sizes. The blur templates with different blur degrees can be used to fit the bokeh effect with different depths (as shown in Fig. 9 (R)). With the all-in-focus image $\mathbf{I}$, its estimated depth map $\mathbf{D}$, and its blur templates $\{\hat{\mathbf{I}}_i\}_{i=1}^N$, the bokeh effect rendering problem can be formulated as

$$\tilde{\mathbf{I}} = \mathcal{B}(\mathbf{I}, \{\hat{\mathbf{I}}_i\}_{i=1}^N, \mathbf{D}), \tag{2}$$

where $\tilde{\mathbf{I}}$ denotes the predicted bokeh image and $\mathcal{B}(\cdot)$ denotes the bokeh effect rendering operation. In a bokeh image, the focused object is clear and sharp while the object out of focus is blurred. Suppose we need to focus on objects in the foreground (as the existing bokeh dataset provided). Then, an intuitive idea is to directly blend the foreground of all-in-focus image $\mathbf{I}$ and the background of blur templates $\{\hat{\mathbf{I}}_i\}_{i=1}^N$. As a result, we can get the final bokeh effect image. To this end, we first pre-process $\mathbf{I}$ and $\{\hat{\mathbf{I}}_i\}_{i=1}^N$ according to the depth map with the following formula to make it easier for the network to learn the fusion weight.

$$\mathbf{I}' = \mathbf{I} \odot \mathbf{D}, \tag{3}$$

$$\hat{\mathbf{I}}'_i = \hat{\mathbf{I}}_i \odot (\mathbf{1} - \mathbf{D}), i \in \{1, 2, \ldots, N\}, \tag{4}$$

where '$\odot$' means the element-wise multiplication, $\mathbf{I}'$ and $\{\hat{\mathbf{I}}'_i\}_{i=1}^N$ denote the images for blending. With the formula (3) and (4), we can generate different $\mathbf{I}'$ and $\{\hat{\mathbf{I}}'_i\}_{i=1}^N$ according to the adjustable depth map, which allows the network to focus on anywhere of the image.

The fusion weight estimation network $\varphi(\cdot)$ takes the depth map $\mathbf{D}$ as input and outputs fusion weight maps $\mathbf{W_A}$ and $\{\mathbf{W_B}_i\}_{i=1}^N$ respectively for $\mathbf{I}'$ and $\{\hat{\mathbf{I}}'_i\}_{i=1}^N$. The fusion weight maps are generated only according to the depth map and are irrelevant to the all-in-focus image, which shows the refocus ability of our method. The formula is

$$\left(\{\mathbf{W_B}_i\}_{i=1}^N, \mathbf{W_A}\right) = \varphi(\mathbf{D}). \tag{5}$$

Here, we rewrite the output in (5) to $\mathbf{W_A} = \varphi(\mathbf{D})_{N+1}$ and

$\{\mathbf{W}_{\mathbf{B}i}\}_{i=1}^{N} = \varphi(\mathbf{D})_{1,\dots,N}$. Then we can rewrite (2) to

$$\tilde{\mathbf{I}} = \mathcal{B}(\mathbf{I}, \{\hat{\mathbf{I}}_i\}_{i=1}^{N}, \mathbf{D}) = \mathbf{W}_{\mathbf{A}} \odot \mathbf{I}' + \sum_{i=1}^{N} \mathbf{W}_{\mathbf{B}i} \odot \hat{\mathbf{I}}'_i \quad (6)$$

$$= \mathbf{W}_{\mathbf{A}} \odot (\mathbf{I} \odot \mathbf{D}) + \sum_{i=1}^{N} \mathbf{W}_{\mathbf{B}i} \odot (\hat{\mathbf{I}}_i \odot (\mathbf{1} - \mathbf{D})) \quad (7)$$

$$= \varphi(\mathbf{D})_{N+1} \odot (\mathbf{I} \odot \mathbf{D}) + \sum_{i=1}^{N} \varphi(\mathbf{D})_i \odot (\hat{\mathbf{I}}_i \odot (\mathbf{1} - \mathbf{D})) \quad (8)$$

Furthermore, since our method renders the bokeh effect by blending all-in-focus image and blur templates with fusion weight map estimated from the depth map, the degree of the bokeh is determined by the degree of the blur templates. That means the degree of the bokeh is adjustable according to our preferences, which is another advantage of our method. The framework is shown in Fig. 2. The network uses an encoder-decoder to estimate the fusion weights for separately processing the all-in-focus image and blur templates in candidate branches and blending them.

Blur template generation $\mathcal{T}(\cdot)$. To synthesize almost realistic bokeh effect by our method, the quality of the blur templates is very important. In general, the bokeh effect can be approximated as applying disk blur on all-in-focus images. However, just rendering with disk blur is still not realistic enough. Compared with the blur effect, a good bokeh effect rendering method should transform a point of light that is blurred as a lens flare. In addition to disk blur, we add an extra gamma correction [8] to simulate this effect.

Given an all-in-focus image $\mathbf{I} \in \mathbb{R}^{H \times W \times 3}$, we aim to generate the blur template $\hat{\mathbf{I}}$ with operation $\mathcal{T}(\cdot)$. To implement function $\mathcal{T}(\cdot)$, ❶ we pad the all-in-focus image $\mathbf{I}$ with kernel size k, where k is the size of disk blur. ❷ we apply gamma correction with gamma value $g(g > 1)$ to make the image appear lighter. ❸ we apply disk blur of kernel size k on the processed image. ❹ we apply inverse gamma correction (*i.e.*, gamma value is $1/g$) on the image. ❺ we unpad the image with kernel size k. The operation of padding and gamma correction are necessary. We show the effectiveness of these two operations in Fig. 3 as an ablation study. As we can see in Fig. 3, disk blur partially reaches the effect of bokeh. Compared with that, the image with disk blur and gamma correction has clear and aesthetically pleasing lens flares, which improves the realistic and aesthetic feeling of the image. However, there exist unnatural artifacts at the edges of the image. That is why we use padding operation to pre-process the image first and unpad it at last. The final result has no unnatural artifacts. We also demonstrate blur templates with different kernel sizes in Fig. 4.

Depth map pre-process. We use Deeplens [48] to generate the depth map $\mathbf{D}$ of the all-in-focus image $\mathbf{I}$. According to our observation, if we use the depth map $\mathbf{D}$ directly, the estimated fusion weight for the blur template image $\hat{\mathbf{I}}$ are small and the bokeh effect is not obvious. We think that it is because of the *distinction* between the depth values of the foreground and background objects in the depth map is not large enough and the depth values of the background objects are too large, which makes the network hard to learn the fusion weight. To increase the difference between foreground and background in the depth map, we design the following process. We first square the values of the depth map to make the values smaller. Then we process the depth map with an operation named $\mathcal{SL}$. $\mathcal{SL}(\cdot)$ is a Sigmoid-like mapping function. The formula is $y = \frac{1}{1+e^{-(x-0.5)*15}}$ and function curve is shown in Fig. 5.

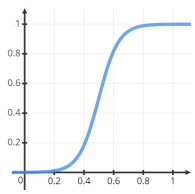

Figure 5. The curve of $\mathcal{SL}(\cdot)$.

Figure 6. The artifacts in the bokeh image that generated without refinement.

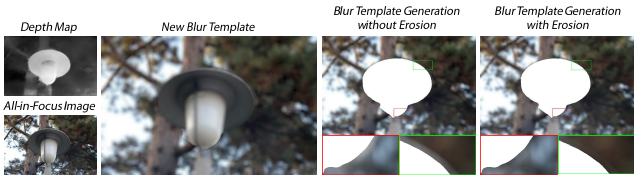

Figure 7. (L-R): top: depth image, bottom: all-in-focus image; new blur template (*i.e.*, blur template with erosion), masked blur template without erosion, masked blur template with erosion. The mask is used to better demonstrate the difference between bokeh images w and w/o erosion.

Refinement with padding and erosion. As shown in Fig. 6, we find that the output has two kinds of artifacts: the artifact in the edge of the image (shown in the yellow box) and the blur effect of the focus area spreads to the out-of-focus area (shown in red box). The solution to the first artifact is the same as dealing with the artifact caused by disk blur when generating a blur template. That is, we use padding and unpadding to deal with this artifact.

For the second artifact, we need to suppress the diffusion blur of the focus area in the blur template according to the depth map. Thus we add erosion operation into the generation of the blur template. To be specific, ❶ in our observation, most of the values of the focus region in the depth map $\mathbf{D}$ are bigger than 0.6. Thus we set the values in the depth map larger than or equal to 0.6 to 1 and values in the depth map smaller than 0.6 to 0 to generate new depth map $\mathbf{D}'$ for distinguishing focused and out-of-focus areas (*i.e.*, $\mathbf{D}'_{i,j} = 1$ if $\mathbf{D}_{i,j} \geq 0.6, \mathbf{D}'_{i,j} = 0$ if $\mathbf{D}_{i,j} < 0.6$, where $\mathbf{D}_{i,j} (1 \leq i \leq H, 1 \leq j \leq W)$ represents the (i,j) location of $\mathbf{D}$). ❷ Generate out-of-focus area $\mathbf{I}_{oof}$ by element-wise multiplying all-in-focus image $\mathbf{I}$ with $(\mathbf{1} - \mathbf{D}')$ (*i.e.*, $\mathbf{I}_{oof} = \mathbf{I} \odot (\mathbf{1} - \mathbf{D}')$). ❸ Set the area that needs to be focused (*i.e.*, the area with value 1 in the depth map) of image $\mathbf{I}$ to be

white color and erode the image to generate erosion image $\mathbf{I}_{ero}$ with kernel size k (*i.e.*, $\mathbf{I}_{i,j} = 255$ if $\mathbf{D'}_{i,j}$ is $1, \mathbf{I}_{ero} = \text{Erosion}(\mathbf{I}, k)$). ❹ Element-wise multiply erosion image $\mathbf{I}_{ero}$ with the depth map $\mathbf{D}'$ to achieve processed focus area $\mathbf{I}_f$ (*i.e.*, $\mathbf{I}_f = \mathbf{I}_{ero} \odot \mathbf{D}'$). ❺ Combine $\mathbf{I}_{oof}$ and $\mathbf{I}_f$ together to achieve image $\mathbf{I}_p$ and apply the blur template generation procedure $\mathcal{T}(\cdot)$ (*i.e.*, $\mathbf{I}_p = \mathbf{I}_f + \mathbf{I}_{oof}, \tilde{\mathbf{I}}_p = \mathcal{T}(\mathbf{I}_p)$). ❻ Apply the blur template generation procedure $\mathcal{T}(\cdot)$ to the all-in-focus image $\mathbf{I}$ (*i.e.*, $\tilde{\mathbf{I}}_b = \mathcal{T}(\mathbf{I})$). ❼ Set the area that needs to be focused (*i.e.*, the area with value 1 in the depth map $\mathbf{D}'$) of image $\mathbf{I}$ to be black color and combine it with $\mathbf{I}_p$ together to obtain the final $\tilde{\mathbf{I}}$ (*i.e.*, $\tilde{\mathbf{I}}_{p_{i,j}} = 0$ if $\mathbf{D'}_{i,j}$ is $1, \tilde{\mathbf{I}} = \tilde{\mathbf{I}}_b + \tilde{\mathbf{I}}_p$). As shown in Fig. 7, we show the new blur template and the difference between blur templates with and without erosion operation. Here we mask the focus area to show the difference better. We can find that the blur template with erosion operation has less diffusion blur of the focus area than the blur template without erosion operation.

Limitation. ❶ Since the blur template generation procedure uses disk blur, thus the generation of blur templates is time-consuming when the kernel size of disk blur is large. ❷ Since the DebsNet is depth-guided, thus the quality of the depth map significantly influences the final bokeh effect. A bad depth map may lead to unnatural bokeh rendering.

4. Proposed Adversarial Bokeh Attack

With the depth-guided bokeh effect rendering method, we aim to reveal the vulnerability of neural networks under the bokeh effect. To attack the neural network, we suggest modifying the depth map instead of directly attacking the rendered bokeh image. Compared with directly applying attacks on the bokeh images, the attack on depth maps will not lead to suspicious noises in the generated bokeh images. The attacks are embedded into the bokeh generation procedure. We take the image classification task as an example to show the degradation of a neural network with our proposed adversarial bokeh attack method. Please note that in the image classification task, the objects that need to be classified are in the foreground under most situations, thus we default setting the foreground as the focus region.

Given a pretrained CNN (*i.e.*, $\phi(\cdot)$) for image classification task, an all-in-focus image $\mathbf{I}$ and its depth map $\mathbf{D}$. We first propose simply applying gradient-based attack on $\phi(\cdot)$ to achieve attacked depth map $\mathbf{D}^* = \mathbf{D} + \delta$ by optimizing the objective function

$$\delta = \arg\max_{\delta^*} \mathcal{J}(\phi(\mathcal{B}(\mathbf{I}, \{\hat{\mathbf{I}}_i\}_{i=1}^N, \mathbf{D} + \delta^*)), y), \quad \text{subject to } \|\delta^*\|_p \leq \epsilon, \tag{9}$$

where $\mathcal{J}(\cdot)$ denotes the cross-entropy loss function with y being the annotation of the all-in-focus image $\mathbf{I}$. By directly applying gradient-based attack on the depth map, although the depth map is with noise, the rendered bokeh images look natural. This method avoids adding suspicious noise in the bokeh image directly by transforming the attack noise in the depth map to the inconspicuous bokeh effect.

However, simply applying a gradient-based attack on the depth map ignores an important characteristic of the bokeh image (*i.e.*, the object in the focus region is clear). With an intuitive idea that the variation in the clear region attracts more attention than variation in a blurred region, we aim to reduce the variation on the focus region and propose a depth-guided gradient-based attack on the depth map. That is, under the assumption that the foreground is the focus region, the attack perturbation on the foreground of the depth map should be smaller than that on the background. We obtain the attacked depth map $\mathbf{D}^* = \mathbf{D} + \delta \odot (\mathbf{1} - \mathbf{D})$ with the same objective as in (9). The depth-guided gradient-based attack brings less variation to the bokeh image while almost maintaining the attack success rate (see §5.4).

Although the noise in the depth map is hidden and becomes imperceptible during the bokeh generation process, we propose a smooth gradient-based attack method to further avoid the influence of the noise and maintain the smoothness of the depth map, which will lead to a more natural bokeh effect. To be specific, we propose to change the value of gradient $\nabla_{\mathbf{D}_{i,j}}$ $(1 \leq i \leq H, 1 \leq j \leq W)$ of depth map $\mathbf{D} \in \mathbb{R}^{H \times W}$ according to its neighbors. The number of neighbors used for reference is depend on l, where l is the kernel size of the smooth function $\mathcal{S}(\cdot)$. In detail, the value $\nabla_{\mathbf{D}_{i,j}}$ is changed according to $\nabla_{\mathbf{D}_{i\pm(l/2),j\pm(l/2)}}$. We obtain the attacked depth map $\mathbf{D}^* = \mathbf{D} + \mathcal{S}(\delta, l)$ with the same objective function in (9).

5. Experiments

We verify the effectiveness of our method from three aspects: the bokeh effect (§5.3), the attack success rate (§5.4), and the improvement to down-stream task (§5.5).

5.1. Target Model

We take two state-of-the-art bokeh effect rendering methods (*i.e.*, DMSHN [5] and PyNET [21]) as the baseline for bokeh effect comparison. For attack task, we take ResNet50 [16], VGG [41], MobileNetV2 [19], and DenseNet [20] as the target model for adversarial attack. We also take other unrestricted attack methods as the baseline to compare the attack performance and image similarity. For potential downstream tasks, we aim to improve the performance of the state-of-the-art defocus deblurring method [25].

5.2. Experimental Setup

Implementation details. We use kernel prediction network (KPN) [32] for implementing the function $\varphi(\cdot)$ to predict

Table 1. Comparison between **DebsNet** and other state-of-the-art bokeh effect rendering methods and the ablation study. The top-1, top-2 and top-3 value of each metric for different types of DebsNet models are colored respectively.

	PyNET	DMSHN	DebsNet-w/o-dm	DebsNet-w-dm	DebsNet-w-pad	DebsNet-w-dp-pad	DebsNet-w-ero-dp-pad
PSNR ↑	20.095	23.2458	20.7692	21.5022	21.4692	20.9719	22.4697
SSIM ↑	0.7469	0.8049	0.7314	0.7485	0.7488	0.7388	0.7603
LPIPS ↓	0.1981	0.1327	0.2103	0.1897	0.1895	0.2213	0.2529

Figure 8. Bokeh effect comparison. The focused objects of "DebsNet-w/o-dm" are blur while they are clear in "DebsNet-w-dm", shows the effectiveness of Formula (3) and (4). Results of "DebsNet-w-pad" have no artifacts in the edge of the images. Compared with results of "DebsNet-w-pad", "DebsNet-w-dp-pad" have more obvious bokeh effect. Compared with results of "DebsNet-w-dp-pad", "DebsNet-w-ero-dp-pad" have less blur diffusion of the focused object. Compared with state-of-the-art bokeh rendering methods PyNET and DMSHN, our method generates bokeh images with more obvious bokeh effect.

the fusion weight maps. The gamma value of the gamma correction is 2.2. We use the Adam [23] with the learning rate of 0.0002 to optimize network parameters. The loss function used by us is L_1 loss. We use one blur template and the variable k of disk blur is 37. The depth map of each all-in-focus image is estimated by using Deeplens [48].

Datasets. There are several datasets involved in our experiment. Ignatov *et al*. [21] open-source the "Everything is Better with Bokeh!" (EBB!) dataset which used in AIM 2020 Bokeh Effect Synthesis Challenge. The dataset contains 4694 pairs of bokeh and bokeh-free images captured using a narrow aperture (f/16) and a high aperture (f/1.8). The resolution of images is around 1024×1536 pixels. This dataset is used by us for the training and testing of the bokeh effect rendering network. We use the NeurIPS-2017 DEV dataset [24] as the testing dataset for the classification task, which contains 1000 ImageNet-like images and is used by NIPS 2017 adversarial attacks and defenses competition. For downstream tasks, we use the dual-pixel defocus deblurring (DPDD) dataset. The DPDD dataset provides 500 dual-pixel images captured a Canon EOS 5D Mark IV.

Metrics. To measure the similarity between prediction and ground truth bokeh images, we use peak signal-to-noise ratio (PSNR), structural similarity [17] (SSIM) and learned perceptual image patch similarity [55] (LPIPS) as the metric. PSNR is the most commonly used measurement for the reconstruction quality of lossy compression. SSIM is used for measuring the similarity between two images. LPIPS is a well-known metric that uses the features of neural networks to judge the similarity of images. Higher means further/more different and lower means more similar. All the experiments were run on an Ubuntu 16.04 system with an Intel(R) Xeon(R) CPU E5-2699 with 196 GB of RAM, with an NVIDIA Tesla V100 GPU of 32G RAM.

Table 2. Comparison of the defocus deblurring performance between IFAN and our finetuned IFAN (*i.e*., F-IFAN).

	PSNR ↑	SSIM ↑	LPIPS ↓
IFAN	25.36620	0.78885	0.21739
F-IFAN (ours)	25.39146	0.78905	0.21946

5.3. Bokeh Effect

Quantitative and qualitative evaluation. In this section, we compare our method to the current two state-of-the-art bokeh rendering methods (*i.e*., DMSHN [5] and PyNET [21]) that were designed and tuned specifically for the considered problem. The quantitative results on comparing with state-of-the-art results and the ablation study are shown in Table 1. In the first row, the "PyNET" and "DMSHN" represent [21] and [5] respectively. "DebsNet-w/o-dm" and "DebsNet-w-dm" mean the DebsNet without using depth map-guided operation introduced in Formula (3), (4) and with depth map-guided operation. We can find that the PSNR, SSIM and LPIPS results of "DebsNet-w-dm" are all higher than "DebsNet-w/o-dm", which means the operation is necessary and make it easier for the network to learn the fusion weight. Please note that "DebsNet-w-dm" is the basic framework proposed by us. Based on "DebsNet-w-dm", we further improve the it with depth map preprocess (*i.e*., "dp"), padding and unpadding refinement (*i.e*., "pad"), erosion refinement (*i.e*., "ero"). We can find that "DebsNet-

w-ero-dp-pad" has the best results in the ablation study. It is also much better than "PyNET" and a bit weaker than "DMSHN". Please note that, contrary to our expectation, neither of the metrics (*i.e.*, PSNR, SSIM, LPIPS) work on the bokeh effect rendering problem. Their values serve only as a rough guide. Thus we have to rely on the actual visual results for further evaluation.

As shown in Fig. 8, the focused objects of "DebsNet-w/o-dm" are blur while they are clear in "DebsNet-w-dm", showing the effectiveness of (3)(4). Results of "DebsNet-w-pad" have no artifacts on the edge of the images. Compared with the results of "DebsNet-w-pad", "DebsNet-w-dp-pad" have more obvious bokeh effect. Compared with the results of "DebsNet-w-dp-pad", "DebsNet-w-ero-dp-pad" have less blur diffusion of the focused object.

In the comparison with the state-of-the-art bokeh rendering methods, we find that they may not generate obvious bokeh effects, which can not wash out unnecessary image details and generate aesthetic images. Furthermore, the degrees of their generated bokeh effect are very similar to the ground truth bokeh images. This phenomenon verifies that they only learn the mapping function according to the training dataset, limiting their flexibility and expansibility.

Refocus ability and adjustable bokeh degree. Compared with other bokeh effect rendering methods, one of the advantages is the refocus ability of our framework. As shown in Fig. 9(L), we can adjust the depth map to determine where to focus. If we set the estimated depth map $\mathbf{D}$ as the input of pre-trained DebsNet, it will focus on the foreground. In contrast, if we use $(\mathbf{1}-\mathbf{D})$ as input, it will focus on the background. The figure shows the refocus ability of our method. We can also use formula $\mathbf{D}=|\mathbf{M}-\mathbf{D}|(0\leq\mathbf{M}\leq 1)$ to modify $\mathbf{D}$ for refocusing on anywhere in the all-in-focus image. Furthermore, by using blur templates with different degrees, we can adjust the bokeh degree of the out-of-focus area. We demonstrate the bokeh degree adjustable results in Fig. 9(R). Here we use the blur template generated by kernel sizes 13, 37, 69 of disk blur to show the bokeh effect of different degrees with the same pre-trained DebsNet. We can find that with a higher degree of blur template, the degree of the bokeh image is higher.

5.4. Adversarial Attack Accuracy

We apply gradient-based attack, depth-guided gradient-based attack, and smooth gradient-based attack on four pre-trained models (ResNet50, VGG, MobileNetV2 and DenseNet) with dataset NeurIPS-2017 DEV. As shown in Table 3, we demonstrate the accuracy of each model to the all-in-focus images (*i.e.*, "all-in-focus" or "aif" for short), bokeh image generated by DebsNet (*i.e.*, "bokeh"), gradient-based attacked bokeh image (*i.e.*, "gda"), depth-guided gradient-based attacked bokeh image (*i.e.*, "dp-gda"), smooth gradient-based attacked bokeh image (*i.e.*, "sm-gda"). Here we use projected gradient descent [31] (PGD) as the gradient-based attack method to attack the bokeh images. For gradient-based attacked bokeh image and depth-guided gradient-based attacked bokeh image, the maximum perturbation for each pixel (*i.e.*, ϵ) is 0.0005, the number of attack iterations is 50. For smooth gradient-based attacked bokeh image, the ϵ is 0.04. We can find that the bokeh image naturally degrades the models (29.7% decrease in average). We also observe this degradation in the result of "PyNET" and "DMSHN", with 50.3% and 36.9% decrease respectively. Compared with the natural degradation, our method significantly decrease the accuracy to almost 0% on all four models. With a similar decrease, we further calculate the image similarity between bokeh images and attacked bokeh images between all-in-focus images. We can find that "dp-gda" always achieve more similar results than "gda". "sm-gda" is a little worse than them. Finally, we compare our method with other state-of-the-art unrestricted attacks (*i.e.*, ColorFool [38] and ACE [56]) on ResNet50. We can find that our method not only generates more similar results to all-in-focus images than other methods but also achieve a higher attack success rate, which shows the effectiveness of our method.

Transferability. We evaluate the attack transferability. As shown in Table 4, the first column shows our attack methods (*i.e.*, gda, dp-gda, sm-gda) and the baselines (*i.e.*, ColorFool and ACE). They all attack the ResNet50 model to obtain attacked images and test them separately on VGG, DenseNet and MobileNetV2. The values are the test accuracy and the lower value means better transferability of the attack method. We can find that our attack method has better attack transferability than ColorFool and ACE.

5.5. Defocus Deblurring Task Improvement

Moreover, the adversarial attacked bokeh images generated by our method can be used for downstream tasks as effective data augmentation. Here we take the state-of-the-art defocus deblurring method IFAN [26] as an example. Our method find hard defocus examples for the defocus deblurring task. The training dataset used by them is DPDD. We use our method to generate adversarial attacked bokeh images according to the training images of DPDD and the same loss of IFAN. Then we collect the attacked images and original training images together to fine-tune the model of IFAN. As shown in Table 2, we compare the IFAN model with our fine-tuned model (*i.e.*, "F-IFAN") on the test dataset of DPDD. We can find that the deblurred images generated by our model achieve higher similarity with the ground truth all-in-focus images than IFAN, which shows the effectiveness of our attack method on improving the defocus deblurring task.

Table 3. The performance of the attack method on four models and the NeurIPS-2017 DEV dataset. The similarity between the attacked bokeh images and the all-in-focus images. "aif" means all-in-focus image. "bokeh" means bokeh image generated by DebsNet. "sm-gda", "gda" and "dp-gda" mean smooth gradient-based attacked bokeh image, gradient-based attacked bokeh image and depth-guided gradient-based attacked bokeh image, respectively. The top-1, top-2 and top-3 value of each metric in each target model is colored respectively. The same values with different colors are actually different, they look the same is due to the limitation of the decimal places.

	ResNet50					***VGG***					***DenseNet***					***MobileNetV2***					***ResNet50***	
	aif	bokeh	sm-gda	gda	dp-gda	aif	bokeh	sm-gda	gda	dp-gda	aif	bokeh	sm-gda	gda	dp-gda	aif	bokeh	sm-gda	gda	dp-gda	ColorFool	ACE
Acc. ↓	0.923	0.638	0.016	0.015	0.015	0.890	0.577	0.019	0.016	0.016	0.946	0.676	0.008	0.008	0.008	0.885	0.565	0.007	0.004	0.004	0.123	0.124
PSNR ↑	\	20.9719	20.6018	20.6771	20.6775	\	20.9719	20.6111	20.6862	20.6862	\	20.9719	20.6058	20.6855	20.6862	\	20.9719	20.6296	20.6842	20.6845	17.32	16.14
SSIM ↑	\	0.7388	0.6715	0.6750	0.6750	\	0.7388	0.6712	0.6752	0.6752	\	0.7388	0.6711	0.6752	0.6752	\	0.7388	0.6719	0.6749	0.6749	0.7457	0.7858
LPIPS ↓	\	0.2213	0.3387	0.3384	0.3384	\	0.2213	0.3375	0.3383	0.3383	\	0.2213	0.3388	0.3383	0.3383	\	0.2213	0.3377	0.3383	0.3383	0.2335	0.2503

Figure 9. (L) Refocus ability, (R) bokeh degree adjustability of *DebsNet*.

Table 4. Attack transferability evaluation. The images are obtained by attacking ResNet50 and test on VGG, DenseNet and MobileNetV2. Lower value means better transferability.

Acc. ↓	***VGG***	***DenseNet***	***MobiNetV2***
bokeh	0.577	0.676	0.565
gda	0.523	0.606	0.512
dp-gda	**0.522**	0.604	0.511
sm-gda	0.524	**0.602**	0.515
ColorFool	0.698	0.838	0.566
ACE	0.545	0.741	**0.453**

6. Conclusions.

In this paper, we propose a depth-guided bokeh synthesis network (DebsNet) which overcomes the defects (*i.e.*, refocus disability and physical unrelated bokeh) of the existing bokeh effect rendering methods. Based on DebsNet, we are able to research the attack feasibility of the bokeh effect on revealing the vulnerability of the neural networks in visual understanding tasks. Furthermore, we demonstrate the usage of the attacked images as the data augmentation for downstream tasks. In the future, we aim to introduce GAN into the framework for more realistic bokeh rendering. Moreover, the proposed AdvBokeh can potentially be used as a supplementary to existing degradation-mimetic adversarial attacks that are not based on additive perturbations, such as adversarial motion blur [12, 13], adversarial weather elements [9, 54], lighting conditions [4, 11, 44, 45], and other attack modalities [3, 10, 14, 28, 49].

A. Appendices

A.1. Visualization of Erosion Refinement

As shown in Fig. 10, to make it easier for understanding, we provide the intermediate products of the erosion refinement procedure. This demonstration will give an intuitive feeling of the refinement procedure proposed by us.

We paste the erosion refinement procedure here for convenience.

To be specific, ❶ in our observation, most of the values of the focus region in the depth map $\mathbf{D}$ are bigger than 0.6. Thus we set the values in the depth map larger than or equal to 0.6 to 1 and values in the depth map smaller than 0.6 to 0 to generate new depth map $\mathbf{D}'$ for distinguishing focused and out-of-focus areas (*i.e.*, $\mathbf{D}'_{i,j} = 1$ if $\mathbf{D}_{i,j} \geq 0.6, \mathbf{D}'_{i,j} = 0$ if $\mathbf{D}_{i,j} < 0.6$, where $\mathbf{D}_{i,j} (1 \leq i \leq H, 1 \leq j \leq W)$ represents the (i,j) location of $\mathbf{D}$). ❷ Generate out-of-focus area $\mathbf{I}_{oof}$ by element-wise multiplying all-in-focus image $\mathbf{I}$ with $(\mathbf{1} - \mathbf{D}')$ (*i.e.*, $\mathbf{I}_{oof} = \mathbf{I} \odot (\mathbf{1} - \mathbf{D}')$). ❸ Set the area that needs to be focused (*i.e.*, the area with value 1 in the depth map) of image $\mathbf{I}$ to be white color and erode the image to generate erosion image $\mathbf{I}_{ero}$ with kernel size k (*i.e.*, $\mathbf{I}_{i,j} = 255$ if $\mathbf{D}'_{i,j}$ is $1, \mathbf{I}_{ero} = \text{Erosion}(\mathbf{I}, k)$). ❹ Element-wise multiply erosion image $\mathbf{I}_{ero}$ with the depth map $\mathbf{D}'$ to achieve processed focus area $\mathbf{I}_f$ (*i.e.*, $\mathbf{I}_f = \mathbf{I}_{ero} \odot \mathbf{D}'$). ❺ Combine $\mathbf{I}_{oof}$ and $\mathbf{I}_f$ together to achieve image $\mathbf{I}_p$ and apply the blur template generation procedure $\mathcal{T}(\cdot)$ (*i.e.*, $\mathbf{I}_p = \mathbf{I}_f + \mathbf{I}_{oof}, \tilde{\mathbf{I}}_p = \mathcal{T}(\mathbf{I}_p)$). ❻ Apply the blur template generation procedure $\mathcal{T}(\cdot)$ to the all-in-focus image $\mathbf{I}$ (*i.e.*,

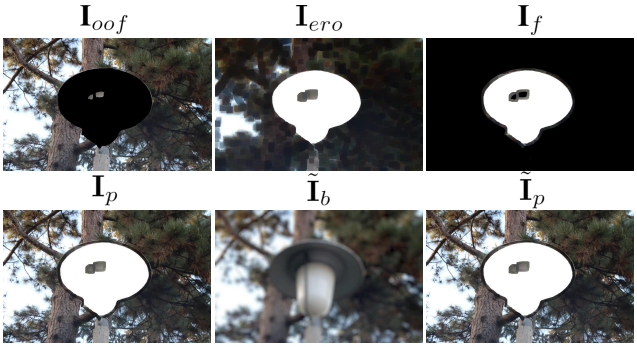

Figure 10. The intermediate products of the erosion refinement procedure.

Table 5. Attack transferability evaluation. The images are obtained by attacking VGG and testing on ResNet50, DenseNet, and MobileNetV2. A lower value means better transferability.

Acc. ↓	ResNet50	DenseNet	MobileNetV2
bokeh	0.638	0.676	0.565
gda	**0.586**	**0.643**	0.507
dp-gda	0.587	0.646	**0.506**
sm-gda	0.592	0.646	0.513
ColorFool	0.659	0.818	0.536
ACE	0.578	0.771	0.512

$\tilde{\mathbf{I}}_b = \mathcal{T}(\mathbf{I})$). ❼ Set the area that needs to be focused (*i.e.*, the area with value 1 in the depth map $\mathbf{D}'$) of image $\mathbf{I}$ to be black color and combine it with $\mathbf{I}_p$ together to obtain the final $\tilde{\mathbf{I}}$ (*i.e.*, $\tilde{\mathbf{I}}_{p_{i,j}} = 0$ if $\mathbf{D}'_{i,j}$ is $1, \tilde{\mathbf{I}} = \tilde{\mathbf{I}}_b + \tilde{\mathbf{I}}_p$).

A.2. Visualization of Comparison with Other Unrestricted Methods

As shown in Fig. 11, we show the comparison of attacked images between our proposed "gda" with other state-of-the-art unrestricted attack methods (*i.e.*, ColorFool [38] and ACE [56]) by attacking ResNet50. We can find that ColorFool and ACE produce very unnatural images. The attacked images not only arouse people's vigilance but also unaesthetic. Compared with them, the attacked images generated by us are more natural and aesthetic.

A.3. Comparison of Transferability

Here we demonstrate the comparison of transferability between our method and other unrestricted methods (*i.e.*, ColorFool [38] and ACE [56]) with the attacked images generated by attacking other three target models (*i.e.*, VGG, DenseNet, MobileNetV2). According to the observation on Table 5, 6 and 7, as well as the Table 4 in the main body, we can find that our proposed attack method has better transferability than ColorFool and ACE on most of the situations.

A.4. Visualization of Improving Defocus Deblurring

As shown in Fig. 12, we show the comparison of the visualization result between IFAN [26] and F-IFAN (*i.e.*, our fine-tuned model). We can find that the fine-tuned model achieves more clear results than IFAN.

Table 6. Attack transferability evaluation. The images are obtained by attacking DenseNet and testing on ResNet50, VGG, and MobileNetV2. A lower value means better transferability.

Acc. ↓	ResNet50	VGG	MobileNetV2
bokeh	0.638	0.577	0.565
gda	0.540	**0.528**	0.514
dp-gda	0.540	0.529	0.515
sm-gda	0.555	0.534	0.521
ColorFool	**0.500**	0.634	**0.455**
ACE	0.551	0.559	0.494

Table 7. Attack transferability evaluation. The images are obtained by attacking MobileNetV2 and testing on ResNet50, VGG, and DenseNet. A lower value means better transferability.

Acc. ↓	ResNet50	VGG	DenseNet
bokeh	0.638	0.577	0.676
gda	0.593	**0.528**	0.634
dp-gda	0.591	**0.528**	0.63
sm-gda	0.587	0.532	**0.628**
ColorFool	0.730	0.742	0.871
ACE	**0.578**	0.556	0.758

References

[1] Rima Alaifari, Giovanni S Alberti, and Tandri Gauksson. Adef: an iterative algorithm to construct adversarial deformations. *arXiv preprint arXiv:1804.07729*, 2018. 3

[2] Anand Bhattad, Min Jin Chong, Kaizhao Liang, Bo Li, and David A Forsyth. Unrestricted adversarial examples via semantic manipulation. *arXiv preprint arXiv:1904.06347*, 2019. 3

[3] Yupeng Cheng, Qing Guo, Felix Juefei-Xu, Xiaofei Xie, Shang-Wei Lin, Weisi Lin, Wei Feng, and Yang Liu. Pasadena: Perceptually Aware and Stealthy Adversarial Denoise Attack. *IEEE Transactions on Multimedia (TMM)*, 2021. 9

[4] Yupeng Cheng, Felix Juefei-Xu, Qing Guo, Huazhu Fu, Xiaofei Xie, Shang-Wei Lin, Weisi Lin, and Yang Liu. Adversarial exposure attack on diabetic retinopathy imagery. *arXiv preprint arXiv:2009.09231*, 2020. 9

[5] Saikat Dutta, Sourya Dipta Das, Nisarg A Shah, and Anil Kumar Tiwari. Stacked deep multi-scale hierarchical network for fast bokeh effect rendering from a single image. In *Proceedings of the IEEE/CVF Conference on Computer Vision and Pattern Recognition*, pages 2398–2407, 2021. 2, 3, 6, 7

[6] Kazuki Endo, Masayuki Tanaka, and Masatoshi Okutomi. Classifying degraded images over various levels of degradation. In *2020 IEEE International Conference on Image Processing (ICIP)*, pages 1691–1695. IEEE, 2020. 1

[7] Logan Engstrom, Brandon Tran, Dimitris Tsipras, Ludwig Schmidt, and Aleksander Madry. Exploring the landscape of

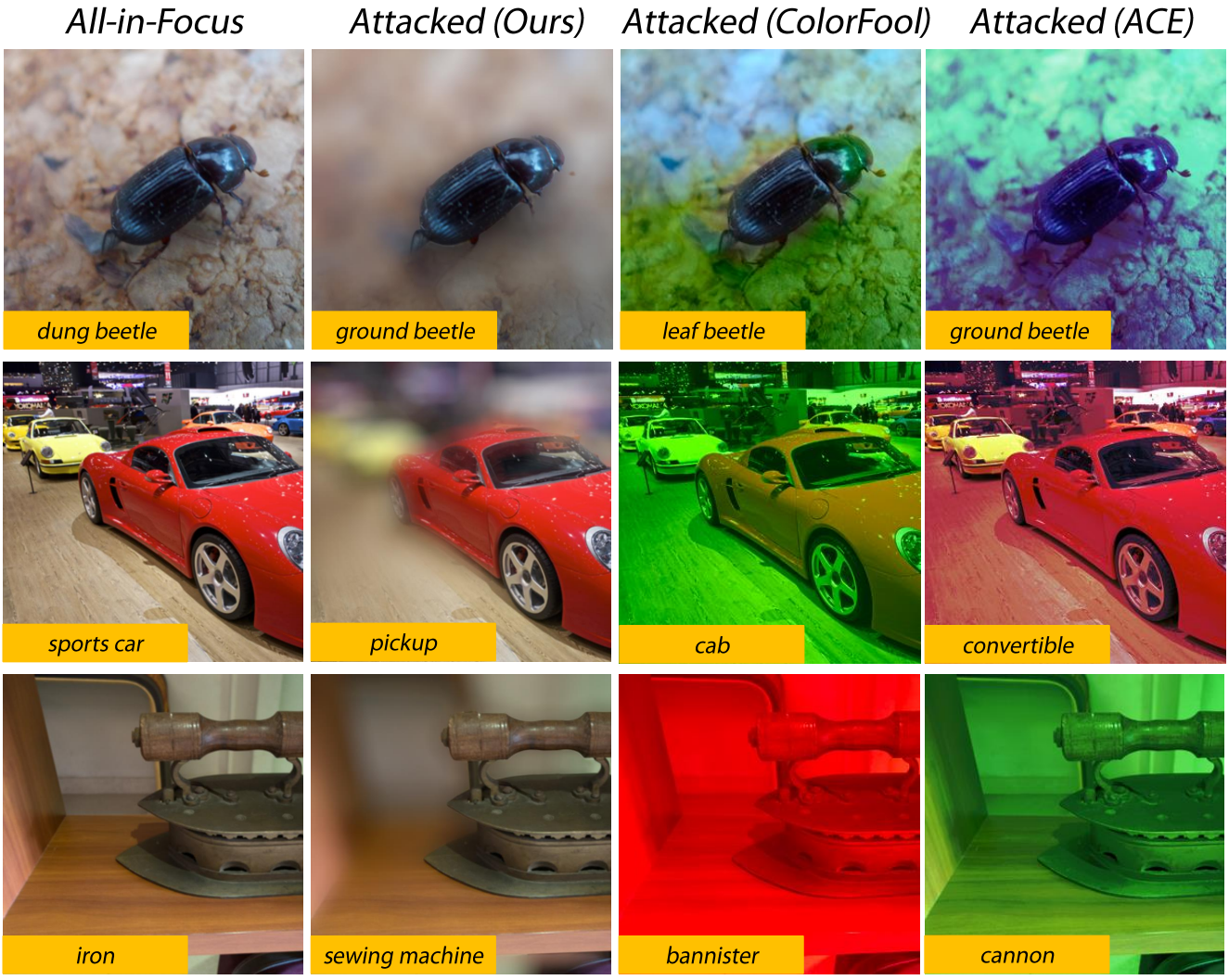

Figure 11. Comparison of attacked images between our proposed "gda" with other state-of-the-art unrestricted attack methods (*i.e.*, ColorFool [38] and ACE [56]) by attacking ResNet50.

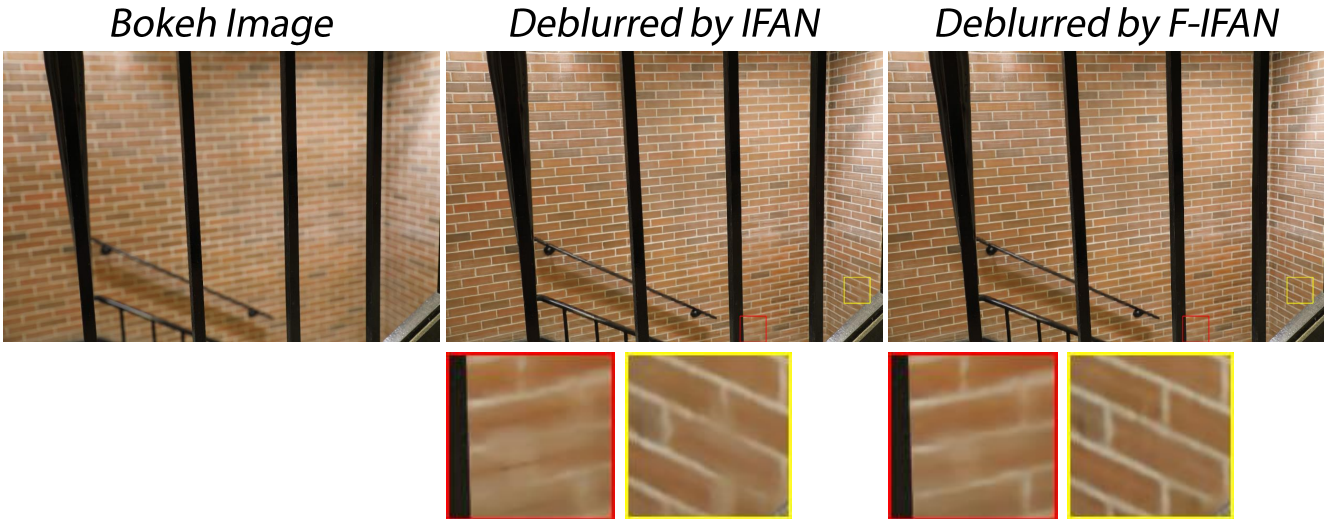

Figure 12. Comparison of the visualization result between IFAN [26] and F-IFAN (*i.e.*, our fine-tuned model).

spatial robustness. In *International Conference on Machine Learning*, pages 1802–1811. PMLR, 2019. 3

[8] Hany Farid. Blind inverse gamma correction. *IEEE transactions on image processing*, 10(10):1428–1433, 2001. 5

[9] Ruijun Gao, Qing Guo, Felix Juefei-Xu, Hongkai Yu, and Wei Feng. AdvHaze: Adversarial Haze Attack. *arXiv preprint arXiv:2104.13673*, 2021. 9

[10] Ruijun Gao, Qing Guo, Felix Juefei-Xu, Hongkai Yu, Xuhong Ren, Wei Feng, and Song Wang. Making images undiscoverable from co-saliency detection. *arXiv preprint arXiv:2009.09258*, 2020. 9

[11] Ruijun Gao, Qing Guo, Qian Zhang, Felix Juefei-Xu, Hongkai Yu, and Wei Feng. Adversarial Relighting against Face Recognition. *arXiv preprint arXiv:2108.07920*, 2021. 9

[12] Qing Guo, Ziyi Cheng, Felix Juefei-Xu, Lei Ma, Xiaofei Xie, Yang Liu, and Jianjun Zhao. Learning to Adversarially Blur Visual Object Tracking. In *Proceedings of the IEEE International Conference on Computer Vision (ICCV)*. IEEE, October 2021. 9

[13] Qing Guo, Felix Juefei-Xu, Xiaofei Xie, Lei Ma, Jian Wang, Bing Yu, Wei Feng, and Yang Liu. Watch out! motion is blurring the vision of your deep neural networks. *arXiv preprint arXiv:2002.03500*, 2020. 3, 9

[14] Qing Guo, Xiaofei Xie, Felix Juefei-Xu, Lei Ma, Zhongguo Li, Wanli Xue, Wei Feng, and Yang Liu. SPARK: Spatial-aware Online Incremental Attack Against Visual Tracking. In *Proceedings of the European Conference on Computer Vision (ECCV)*, Aug 2020. 9

[15] Paul Haeberli and Kurt Akeley. The accumulation buffer: Hardware support for high-quality rendering. *ACM SIGGRAPH computer graphics*, 24(4):309–318, 1990. 3

[16] Kaiming He, Xiangyu Zhang, Shaoqing Ren, and Jian Sun. Deep residual learning for image recognition. In *Proceedings of the IEEE conference on computer vision and pattern recognition*, pages 770–778, 2016. 6

[17] Alain Hore and Djemel Ziou. Image quality metrics: Psnr vs. ssim. In *2010 20th international conference on pattern recognition*, pages 2366–2369. IEEE, 2010. 7

[18] Hossein Hosseini and Radha Poovendran. Semantic adversarial examples. In *Proceedings of the IEEE Conference on Computer Vision and Pattern Recognition Workshops*, pages 1614–1619, 2018. 3

[19] Andrew G Howard, Menglong Zhu, Bo Chen, Dmitry Kalenichenko, Weijun Wang, Tobias Weyand, Marco Andreetto, and Hartwig Adam. Mobilenets: Efficient convolutional neural networks for mobile vision applications. *arXiv preprint arXiv:1704.04861*, 2017. 6

[20] Gao Huang, Zhuang Liu, Laurens Van Der Maaten, and Kilian Q Weinberger. Densely connected convolutional networks. In *Proceedings of the IEEE conference on computer vision and pattern recognition*, pages 4700–4708, 2017. 6

[21] Andrey Ignatov, Jagruti Patel, and Radu Timofte. Rendering natural camera bokeh effect with deep learning. In *Proceedings of the IEEE/CVF Conference on Computer Vision and Pattern Recognition Workshops*, pages 418–419, 2020. 2, 3, 6, 7

[22] Andrey Ignatov, Jagruti Patel, Radu Timofte, Bolun Zheng, Xin Ye, Li Huang, Xiang Tian, Saikat Dutta, Kuldeep Purohit, Praveen Kandula, et al. Aim 2019 challenge on bokeh effect synthesis: Methods and results. In *2019 IEEE/CVF International Conference on Computer Vision Workshop (ICCVW)*, pages 3591–3598. IEEE, 2019. 2

[23] Diederik P Kingma and Jimmy Ba. Adam: A method for stochastic optimization. *arXiv preprint arXiv:1412.6980*, 2014. 7

[24] Alexey Kurakin, Ian Goodfellow, Samy Bengio, Yinpeng Dong, Fangzhou Liao, Ming Liang, Tianyu Pang, Jun Zhu, Xiaolin Hu, Cihang Xie, et al. Adversarial attacks and defences competition. In *The NIPS'17 Competition: Building Intelligent Systems*, pages 195–231. Springer, 2018. 7

[25] Junyong Lee, Hyeongseok Son, Jaesung Rim, Sunghyun Cho, and Seungyong Lee. Iterative filter adaptive network for single image defocus deblurring. In *Proceedings of the IEEE/CVF Conference on Computer Vision and Pattern Recognition*, pages 2034–2042, 2021. 6

[26] Junyong Lee, Hyeongseok Son, Jaesung Rim, Sunghyun Cho, and Seungyong Lee. Iterative filter adaptive network for single image defocus deblurring. In *The IEEE Conference on Computer Vision and Pattern Recognition (CVPR)*, June 2021. 8, 10, 11

[27] Sungkil Lee, Elmar Eisemann, and Hans-Peter Seidel. Real-time lens blur effects and focus control. *ACM Transactions on Graphics (TOG)*, 29(4):1–7, 2010. 3

[28] Yiming Li, Congcong Wen, Felix Juefei-Xu, and Chen Feng. Fooling LiDAR Perception via Adversarial Trajectory Perturbation. In *Proceedings of the IEEE International Conference on Computer Vision (ICCV)*. IEEE, October 2021. 9

[29] Sifei Liu, Shalini De Mello, Jinwei Gu, Guangyu Zhong, Ming-Hsuan Yang, and Jan Kautz. Learning affinity via spatial propagation networks. *arXiv preprint arXiv:1710.01020*, 2017. 3

[30] Jonathan Long, Evan Shelhamer, and Trevor Darrell. Fully convolutional networks for semantic segmentation. In *Proceedings of the IEEE conference on computer vision and pattern recognition*, pages 3431–3440, 2015. 3

[31] Aleksander Madry, Aleksandar Makelov, Ludwig Schmidt, Dimitris Tsipras, and Adrian Vladu. Towards deep learning models resistant to adversarial attacks. *arXiv preprint arXiv:1706.06083*, 2017. 8

[32] Ben Mildenhall, Jonathan T Barron, Jiawen Chen, Dillon Sharlet, Ren Ng, and Robert Carroll. Burst denoising with kernel prediction networks. In *Proceedings of the IEEE Conference on Computer Vision and Pattern Recognition*, pages 2502–2510, 2018. 6

[33] Yanting Pei, Yaping Huang, Qi Zou, Xingyuan Zhang, and Song Wang. Effects of image degradation and degradation removal to cnn-based image classification. *IEEE transactions on pattern analysis and machine intelligence*, 2019. 1

[34] Kuldeep Purohit, Maitreya Suin, Praveen Kandula, and Rajagopalan Ambasamudram. Depth-guided dense dynamic filtering network for bokeh effect rendering. In *2019 IEEE/CVF International Conference on Computer Vision Workshop (ICCVW)*, pages 3417–3426. IEEE, 2019. 2, 3

[35] Ming Qian, Congyu Qiao, Jiamin Lin, Zhenyu Guo, Chenghua Li, Cong Leng, and Jian Cheng. Bggan: Bokeh-glass generative adversarial network for rendering realistic bokeh. In *European Conference on Computer Vision*, pages 229–244. Springer, 2020. 2

[36] Mohamed Sayed and Gabriel Brostow. Improved handling of motion blur in online object detection. In *Proceedings of the IEEE/CVF Conference on Computer Vision and Pattern Recognition*, pages 1706–1716, 2021. 1

[37] M Ibrahim Sezan, Gordana Pavlovic, A Murat Tekalp, and A Tanju Erdem. On modeling the focus blur in image restoration. In *ICASSP*, volume 91, pages 2485–2488, 1991. 4

[38] Ali Shahin Shamsabadi, Ricardo Sanchez-Matilla, and Andrea Cavallaro. Colorfool: Semantic adversarial colorization. In *Proceedings of the IEEE/CVF Conference on Computer Vision and Pattern Recognition*, pages 1151–1160, 2020. 3, 8, 10, 11

[39] Xiaoyong Shen, Aaron Hertzmann, Jiaya Jia, Sylvain Paris, Brian Price, Eli Shechtman, and Ian Sachs. Automatic portrait segmentation for image stylization. *Computer Graphics Forum*, 35(2):93–102, 2016. 2, 3

[40] Xiaoyong Shen, Xin Tao, Hongyun Gao, Chao Zhou, and Jiaya Jia. Deep automatic portrait matting. In *European conference on computer vision*, pages 92–107. Springer, 2016. 2, 3

[41] Karen Simonyan and Andrew Zisserman. Very deep convolutional networks for large-scale image recognition. *arXiv preprint arXiv:1409.1556*, 2014. 6

[42] Cyril Soler, Kartic Subr, Frédo Durand, Nicolas Holzschuch, and François Sillion. Fourier depth of field. *ACM Transactions on Graphics (TOG)*, 28(2):1–12, 2009. 3

[43] Nguyen Hieu Thao, Oleg Soloviev, Jacques Noom, and Michel Verhaegen. Nonuniform defocus removal for image classification. *arXiv preprint arXiv:2106.13864*, 2021. 1

[44] Binyu Tian, Qing Guo, Felix Juefei-Xu, Wen Le Chan, Yupeng Cheng, Xiaohong Li, Xiaofei Xie, and Shengchao Qin. Bias Field Poses a Threat to DNN-Based X-Ray Recognition. In *IEEE International Conference on Multimedia and Expo (ICME)*, 2021. 9

[45] Binyu Tian, Felix Juefei-Xu, Qing Guo, Xiaofei Xie, Xiaohong Li, and Yang Liu. AVA: Adversarial Vignetting Attack against Visual Recognition. In *Proceedings of the International Joint Conference on Artificial Intelligence (IJCAI)*, 2021. 9

[46] Igor Vasiljevic, Ayan Chakrabarti, and Gregory Shakhnarovich. Examining the impact of blur on recognition by convolutional networks. *arXiv preprint arXiv:1611.05760*, 2016. 1

[47] Neal Wadhwa, Rahul Garg, David E Jacobs, Bryan E Feldman, Nori Kanazawa, Robert Carroll, Yair Movshovitz-Attias, Jonathan T Barron, Yael Pritch, and Marc Levoy. Synthetic depth-of-field with a single-camera mobile phone. *ACM Transactions on Graphics (ToG)*, 37(4):1–13, 2018. 2, 3

[48] Lijun Wang, Xiaohui Shen, Jianming Zhang, Oliver Wang, Zhe Lin, Chih-Yao Hsieh, Sarah Kong, and Huchuan Lu. Deeplens: Shallow depth of field from a single image. *arXiv preprint arXiv:1810.08100*, 2018. 2, 3, 4, 5, 7

[49] Run Wang, Felix Juefei-Xu, Qing Guo, Yihao Huang, Xiaofei Xie, Lei Ma, and Yang Liu. Amora: Black-box Adversarial Morphing Attack. In *Proceedings of the ACM International Conference on Multimedia (ACM MM)*, 2020. 9

[50] Jiaze Wu, Changwen Zheng, Xiaohui Hu, Yang Wang, and Liqiang Zhang. Realistic rendering of bokeh effect based on optical aberrations. *The Visual Computer*, 26(6):555–563, 2010. 3

[51] Chaowei Xiao, Jun-Yan Zhu, Bo Li, Warren He, Mingyan Liu, and Dawn Song. Spatially transformed adversarial examples. *arXiv preprint arXiv:1801.02612*, 2018. 3

[52] Xiangyu Xu, Deqing Sun, Sifei Liu, Wenqi Ren, Yu-Jin Zhang, Ming-Hsuan Yang, and Jian Sun. Rendering portraitures from monocular camera and beyond. In *Proceedings of the European Conference on Computer Vision (ECCV)*, pages 35–50, 2018. 2, 3

[53] Xuan Yu, Rui Wang, and Jingyi Yu. Real-time depth of field rendering via dynamic light field generation and filtering. *Computer Graphics Forum*, 29(7):2099–2107, 2010. 3

[54] Liming Zhai, Felix Juefei-Xu, Qing Guo, Xiaofei Xie, Lei Ma, Wei Feng, Shengchao Qin, and Yang Liu. It's raining cats or dogs? adversarial rain attack on dnn perception. *arXiv preprint arXiv:2009.09205*, 2020. 9

[55] Richard Zhang, Phillip Isola, Alexei A Efros, Eli Shechtman, and Oliver Wang. The unreasonable effectiveness of deep features as a perceptual metric. In *Proceedings of the IEEE conference on computer vision and pattern recognition*, pages 586–595, 2018. 7

[56] Zhengyu Zhao, Zhuoran Liu, and Martha Larson. Adversarial color enhancement: Generating unrestricted adversarial images by optimizing a color filter. *arXiv preprint arXiv:2002.01008*, 2020. 3, 8, 10, 11

[57] Shuai Zheng, Sadeep Jayasumana, Bernardino Romera-Paredes, Vibhav Vineet, Zhizhong Su, Dalong Du, Chang Huang, and Philip HS Torr. Conditional random fields as recurrent neural networks. In *Proceedings of the IEEE international conference on computer vision*, pages 1529–1537, 2015. 3